Published in final edited form as:
Magn Reson Med. 2013 November ; 70(5): . doi:10.1002/mrm.24571.

Characterizing Inter-Compartmental Water Exchange in Myelinated Tissue using Relaxation Exchange Spectroscopy

Richard D. Dortch[a,b], **Kevin D. Harkins**[a,b], **Meher R. Juttukonda**[c], **John C. Gore**[a,b,c,e,f], and **Mark D. Does**[a,b,c,d]

[a]Department of Radiology and Radiological Sciences, Vanderbilt University, Nashville, TN, USA

[b]Vanderbilt University Institute of Imaging Science, Vanderbilt University, Nashville, TN, USA

[c]Department of Biomedical Engineering, Vanderbilt University, Nashville, TN, USA

[d]Department of Electrical Engineering, Vanderbilt University, Nashville, TN, USA

[e]Department of Physics and Astronomy, Vanderbilt University, Nashville, TN, USA

[f]Department of Molecular Physiology and Biophysics, Vanderbilt University, Nashville, TN, USA

Abstract

Purpose—To investigate inter-compartmental water exchange in two model myelinated tissues *ex vivo* using relaxation exchange spectroscopy (REXSY).

Methods—Building upon a previously developed theoretical framework, a three-compartment (myelin, intra-axonal, and extra-axonal water) model of the inversion-recovery prepared REXSY signal was applied in excised rat optic nerve and frog sciatic nerve samples to estimate the water residence time constants in myelin (τ_{myelin}).

Results—In the rat optic nerve samples, τ_{myelin} = 138 ± 15 ms (mean ± standard deviation) was estimated. In sciatic nerve, which possesses thicker myelin sheaths than optic nerve, a much longer τ_{myelin} = 2046 ± 140 ms was observed.

Conclusions—Consistent with previous studies in rat spinal cord, the extrapolation of exchange rates in optic nerve to *in vivo* conditions indicates that τ_{myelin} < 100 ms. This suggests that there is a significant effect of inter-compartmental water exchange on the transverse relaxation of water protons in white matter. The much longer τ_{myelin} values in sciatic nerve supports the postulate that the inter-compartmental water exchange rate is mediated by myelin thickness. Together, these findings point to the potential for MRI methods to probe variations in myelin thickness in white matter.

Keywords

water exchange; diffusion; exchange spectroscopy; T_2; myelin thickness; myelin water fraction

INTRODUCTION

The transverse relaxation of water protons in nerve and white matter is multiexponential and typically characterized by two or three signal components: (*i*) a short transverse relaxation time constant (T_2) component arising predominantly from water between myelin bilayers (i.e., myelin water) and (*ii*) one or two longer-T_2 components arising predominantly from

Please send correspondence to: Correspondence to: Mark D. Does, Ph.D., 1161 21st Ave South, AA-1105 MCN, Nashville, TN 37232-2310, mark.does@vanderbilt.edu.

water within and between axons (i.e., nonmyelin water) (1–3). The fractional contribution of the short-T_2 water signal to the total signal is known as the myelin water fraction (MWF). Previous work has demonstrated that the MWF reports on myelin content (4, 5); however, it is also sensitive to the rate of inter-compartmental water exchange, which has been predicted to vary as a function of axon diameter and myelin thickness (6, 7). Thus, the exact relationship between MWF and myelin volume fraction, and, more generally, between the spectrum of water proton T_2s (T_2 spectrum) and neuronal microstructure remains undefined.

Previous attempts to characterize inter-compartmental water exchange in myelinated tissues used two-dimensional (2D) magnetization transfer (MT)–T_2 measurements (8–10). The resulting data were fitted to a four-pool model (myelin and nonmyelin water and two associated macromolecular (MM) proton pools) that included exchange between the water pools and between the water and MM pools. Such studies are challenging because of the large number of free and covarying parameters, particularly when MT and water exchange rates are of similar magnitude. Therefore, it is not surprising that these studies resulted in widely varied estimates of the mean water residence in myelin (τ_{myelin})—160 to 310 ms *ex vivo* at bore temperature (8, 9) and 280 to 780 ms *in vivo* (10).

A potentially more direct approach to measuring inter-compartmental water exchange is through relaxation exchange spectroscopy (REXSY) (11, 12). With REXSY, the presence of inter-compartmental water exchange during a mixing period is directly observed as off-diagonal components in a 2D T_2–T_2 relaxation spectrum; and the evolution of these off-diagonal peaks is sensitive to the rate of inter-compartmental water exchange. Thus, it is possible to estimate exchange rates by acquiring 2D REXSY data over a range of mixing times, although this results in a long, 3D experiment. In cases where apparent T_1 differences exist between water pools, a more expedient method (IR-REXSY) uses an inversion-recovery (IR) magnetization preparation to reduce the acquisition from three to two dimensions (13). To date, REXSY-based methods have been used to study water dynamics in porous media (14–17), model chemical systems (11, 13), and hydrated elastin (18), but not yet intact tissues. In this study, relaxation exchange spectroscopy was applied to the study of inter-compartmental water exchange in freshly excised rat optic nerves and frog sciatic nerves, two model myelinated tissues with different mean myelin sheath thickness. Because these studies were performed in freshly excised samples, the more expedient IR-REXSY approach was employed.

THEORY

A detailed description of relaxation exchange spectroscopy methods, including IR-REXSY has been published previously (13). Here, the IR-REXSY method is briefly summarized. The IR-REXSY sequence (Fig. 1) involves an IR preparation period of duration t_I designed to approximately null of the longitudinal magnetization of one signal T_2-component; an excitation and pre-storage delay of duration t_{E1}; a storage period of duration t_M to allow mixing of water between compartments; and a readout out using a Carr-Purcell-Meiboom-Gill (CPMG) measurement (19, 20). The sequence is repeated over a range of t_M values, resulting in 2D experiment—number of CPMG echoes *(NE)* × number of t_M values (*NM*). Note that the phase-cycled excitation between the IR and storage periods subtracts the magnetization from acquisitions stored on the $\pm z$-axis during the mixing period and is employed to ensure that the signal acquired during the CPMG readout arises solely from spins that are excited by the first π/2 pulse. Therefore, any growth in the magnitude of the IR-suppressed signal component during the mixing period is directly attributable to exchange with the non-suppressed component(s).

To quantitatively analyze NMR data from multiple exchanging compartments, consider N exchanging water compartments defined by unique equilibrium magnetizations $M_{0,i}$ (i = 1 to N), longitudinal and transverse relaxation rate constants $R_{1,i}$ and $R_{2,i}$ (or time constants $T_{1,i}$ and $T_{2,i}$), and inter-compartmental exchange rate constants k_{ij}. Note that k_{ij} represents the rate constant of exchange from compartment i to compartment j (j = 1 to N, $j \neq i$), and under the principle of detailed balance, $k_{ij}M_{0,i} = k_{ji}M_{0,j}$. If the compartments are assumed to be well-mixed at all times (see *Discussion*), the Bloch-McConnell (21) equations can be solved to provide a signal equation for a given pulse sequence during free precession. For a CPMG measurement acquired at equilibrium with a perfect 90° excitation, the signal equation is

$$S_{\mathrm{CPMG}}(t_{\mathrm{E},m}) = \mathbf{1}_{1\times N} \exp\left(\mathbf{L}_2 t_{\mathrm{E},m}\right) \mathbf{M}_0, \quad [1]$$

where $t_{\mathrm{E},m}$ (m = 1 to NE) is the echo time, $\mathbf{1}_{1\times N}$ is 1 × N vector of ones, $\mathbf{M}_0$ is a N × 1 column vector of compartmental equilibrium magnetizations, and $\mathbf{L}_2$ is a N × N matrix defined as

$$\mathbf{L}_2 = \begin{pmatrix} -R_{2,1} - \sum_{i\neq 1} k_{1i} & \square & k_{N1} \\ \vdots & \ddots & \vdots \\ k_{1N} & \cdots & -R_{2,N} - \sum_{i\neq N} k_{Ni} \end{pmatrix}. \quad [2]$$

Reducing the matrix exponential in Eq. [1] by expanding $\mathbf{L}_2$ in terms of its eigenvalues and eigenvectors yields

$$S_{\mathrm{CPMG}}(t_{\mathrm{E},m}) = \mathbf{1}_{1\times N}\mathbf{U} \begin{pmatrix} \exp\left(-\lambda_1 t_{\mathrm{E},m}\right) & \square & 0 \\ \vdots & \ddots & \vdots \\ 0 & \cdots & \exp\left(-\lambda_N t_{\mathrm{E},m}\right) \end{pmatrix} \mathbf{U}^{-1}\mathbf{M}_0, \quad [3]$$

where λ_i is the i^{th} eigenvalue of $\mathbf{L}_2$ and $\mathbf{U}$ is a matrix whose columns are the corresponding eigenvectors.

From this equation, it can be seen that the magnetization from each pool, and thus also the total signal, evolves as a sum of N exponentials terms with observed transverse relaxation time constants $\mathbf{T}_{2\mathrm{obs}}$, where $T_{2\mathrm{obs},i} = -1/\lambda_i$. Given a sampling of $S_{\mathrm{CPMG}}(t_{\mathrm{E},m})$ with sufficient signal-to-noise ratio (SNR) over a suitable number/range of t_{E} values, it is possible to estimate these $T_{2\mathrm{obs},i}$ terms and corresponding signal component amplitudes $P_{\mathrm{CPMG},i}$ using a numerical inverse Laplace transform (ILT) algorithm (e.g., (22, 23)). Factoring Eq. [3] with respect to each exponential term, one can obtain a relationship between model parameters (in $\mathbf{M}_0$ and $\mathbf{L}_2$) and these observed signal component amplitudes

$$\mathbf{P}_{\mathrm{CPMG}} = \left(\mathbf{U}^{-1}\mathbf{M}_0\right) \circ \left(\mathbf{1}_{1\times N}\,\mathbf{U}\right)^{\mathrm{T}}. \quad [4]$$

Here $\mathbf{P}_{\mathrm{CPMG}}$ is a N × 1 vector of component amplitudes ($P_{\mathrm{CPMG},i}$) derived from the ILT of $S_{\mathrm{CPMG}}(t_{\mathrm{E},m})$, ○ represents the element-wise (or Hadamard) matrix multiplication operation, and $^{\mathrm{T}}$ represents the matrix transpose operation.

From a similar approach, the signal equation for the IR-REXSY sequence is

$$S_{IREX}(t_{\mathrm{E},m}, t_{\mathrm{M},n}) = 21_{1\times N} \exp\left(\mathbf{L}_2 t_{\mathrm{E},m}\right) \exp\left(\mathbf{L}_1 t_{\mathrm{M},n}\right) \exp\left(\mathbf{L}_2 t_{\mathrm{E1}}\right) \left[2\exp\left(\mathbf{L}_1 t_1\right) \mathbf{M}_0 - \mathbf{M}_0\right], \quad [5]$$

where $t_{\mathrm{E},m}$ is defined as above, $t_{\mathrm{M},n}$ (n = 1 to NM) is the mixing time, t_{E1} is the pre-storage echo time, and $\mathbf{L}_1$ is defined similarly to $\mathbf{L}_2$ (Eq. [2]) except with compartment longitudinal relaxation rate constants ($R_{1,i}$) in place of the transverse relaxation rate constants ($R_{2,i}$). Note that this signal equation assumes the previously mentioned two-part phase cycle, which subtracts the magnetization from acquisitions stored on the ±z-axis (the factor of 2 in Eq. [5] accounts for this, see Fig. 1 for details). Again, the matrix exponential terms dependent on t_{E} can be expanded and then the equation can be factored with respect to the resulting apparent transverse relaxation rate terms, resulting in

$$\mathbf{P}_{\mathrm{IREX}}(t_{\mathrm{M},n}) = 2\left\{\left(\mathbf{U}^{-1} \exp\left(\mathbf{L}_1 t_{\mathrm{M},n}\right) \exp\left(\mathbf{L}_2 t_{\mathrm{E1}}\right) \left[2\exp\left(\mathbf{L}_1 t_1\right) \mathbf{M}_0 - \mathbf{M}_0\right]\right)\right\} \circ \left[\mathbf{1}_{1\times N} \mathbf{U}\right]^{\mathrm{T}}, \quad [6]$$

where $\mathbf{P}_{\mathrm{IREX}}(t_{\mathrm{M},n})$ is $N \times 1$ vector of component amplitudes derived from the 1D ILT of $S_{\mathrm{IREX}}(t_{\mathrm{M}}, t_{\mathrm{E}})$ with respect to t_{E} at each t_{M} value. In other words, it describes the evolution of the apparent component amplitudes with respect to t_{M}.

In the context of myelinated tissues, the microstructures of both sciatic and optic nerve suggest the need for a three-compartment model of water: water in-between myelin bilayers (myelin water), water in the axoplasm (intra-axonal), and water in outside of myelinated axons (extra-axonal). Sciatic nerve NMR relaxometry has long been known to exhibit three distinct T_2 components (1), which current literature assigns to myelin, extra-axonal, and intra-axonal water in order of increasing relaxation time (24–26). The interpretation of a shorter T_2 of extra-axonal compared with intra-axonal water, which may be counter-intuitive, is based on observations of water diffusion (24) and contrast-agent effects (25, 26) on the water T_2 spectrum of nerve, and is likely due to the abundance of collagen in peripheral nerve, as noted by Peled *et al.* (23). In contrast, most previous studies of white matter (3–6, 26) and optic nerve (8, 26, 27) have identified two T_2 components, although at least one study has identified three T_2 components in optic nerve (28). Consequently, the present study uses a three-compartment model for sciatic nerve and investigates both two- and three-compartment models for optic nerve. To simplify the three-compartment models, it is assumed that no exchange occurs directly between intra- and extra-axonal water. That is, water must traverse the myelin sheath to travel between the intra- and extra-axonal spaces. For the analysis herein, we arbitrarily label each of the three nerve water compartments as i □ [a, b, c], where ‘a’, ‘b’ and ‘c’ represent signal from components in order of increasing T_2. As summarized in Fig. 2, this results in a model with 11 independent parameters: three equilibrium magnetizations ($M_{0,\mathrm{a/b/c}}$), three each longitudinal and transverse relaxation time constants ($T_{1,\mathrm{a/b/c}}$ and $T_{2,\mathrm{a/b/c}}$), and two exchange rate constants (k_{ab} and k_{ac}).

METHODS

Sample Preparation

Adult male rats (Sprague-Dawley) and African clawed frogs (*Xenopus laevis*) were used for all studies in accordance with protocols approved by the Institutional Animal Care and Use Committee of Vanderbilt University. Rats (n = 5, 432 ± 64 grams) were euthanized via CO_2 inhalation. Following euthanasia, both optic nerves were excised from the optic chiasm to the skull (≈1 cm segments), cleaned of attached blood and soft tissue, and immersed in phosphate buffered saline (PBS; Mediatech Inc., Herdon, VA) at room temperature until NMR was performed. Frogs (n = 4, 143 ± 22 grams) were euthanized by immersion in a 10 g/L bath of tricaine methanesulfonate (Finquel®; Argent, Redmond, WA) for 20–30

minutes. Following euthanasia, a 1–2 cm segment of sciatic nerve were excised from one hindlimb, cleaned of attached blood and soft tissue, and immersed in amphibian Ringer's solution (Fisher Scientific, Rochester, NY) at room temperature until NMR was performed.

Prior to each NMR session, the nerve sample was patted dry to remove extraneous fluid, placed in a 5-mm NMR tube, and bathed in perfluorcarbon solution (Fomblin®; Solvay Solexis, Thorofare, NJ) to prevent tissue drying without contributing proton signal. NMR measurements were immediately performed as described in the following section. The total time from euthanasia until the end of the NMR experiments was approximately two hours. To test for relevant changes in tissue microanatomy during this period, CPMG measurements (see below) were made at the beginning and end of each NMR session.

Following NMR, one optic and one sciatic nerve sample were processed for light microscopy. To do so, samples were fixed by immersion in 0.5% paraformaldehyde/4% glutaraldehyde in buffer (0.1 M phosphate buffer for rat optic nerve and Amphibian Ringer's solution for frog sciatic nerve), post-fixed in osmium tetroxide, and embedded in Epon. From these blocks, sections (1 μm thick) were cut, stained with toluidine blue, and evaluated by light microscopy on an Olympus BX41 microscope equipped with an Optronics Microfire digital camera. Fields at 40× and 100× were photographed for sciatic and optic nerve, respectively. Axon diameters and myelin sheath thicknesses were manually measured in these sections as described previously (6).

Data Acquisition

NMR measurements were performed on freshly excised nerve samples at bore temperature (≈20°C). Sciatic nerve samples were scanned on a 4.7-T (200 MHz), 31-cm bore Varian/Agilent (Santa Clara, CA) Direct Drive MRI system, while the smaller optic nerve samples were scanned on a 9.4-T (400 MHz), 16-cm bore (same console type). An in-house-built loop-gap resonator (29) was used for RF transmission and reception at both field strengths. One sciatic nerve and three optic nerve samples were scanned at both field strengths to test for a systemic difference between systems.

Data were collected with CPMG [$S_{CPMG}(t_{E,m})$, $m = 1$ to NE] and IR-REXSY [$S_{IREX}(t_{E,m}, t_{M,n})$, $m = 1$ to NE, $n = 1$ to NM] pulse sequences. All measurements used $NE = 1024$ and an echo spacing (Δt_E) of 1 ms. The predelay (t_D) was set long enough to ensure magnetization had returned to equilibrium [8/12 s (optic/sciatic nerve, IR-REXSY) or 15 s (CPMG)], and 4 to 16 excitations were averaged to ensure adequate SNR. Because IR-REXSY model does not require perfect myelin water signal nulling and a short study time was needed to accommodate the fresh tissue samples, t_I was quickly set to approximately null the myelin water T_2 component as measured from IR-CPMG acquisitions over a few t_I values. Using this t_I value and a $t_{E1} = 2$ ms, IR-REXSY data were collected $NM = 16$ or 20 t_M values logarithmically spaced between 10–15 ms and 2 s. For all experiments, the RF pulses were carefully calibrated by pulse width adjustment, resulting in ≈ 10 μs and ≈ 20 μs durations for 90° and 180° hard pulses, respectively.

Data Analysis

All data were processed using MATLAB (The Mathworks, Natick, MA). The first five echoes of each measurement were discarded to avoid previously observed signal components with $T_2 \approx 1$ ms (30), and echoes beyond $t_E = 350$ ms for optic nerve and $t_E = 800$ ms for sciatic nerve (≈ 4× the longest respective nerve T_2 components) were discarded to minimize the impact of Rician noise (31) as the decay approached the noise floor, which was especially important in analyzing the lower-SNR IR-REXSY data. In order to utilize Eqs. [4] and [6], which relate the T_2 spectral component amplitudes and mean T_2s to

intrinsic model parameters, both S_{CPMG} and S_{IREX} signals were transformed from the echo-time domain to the T_2 domain. In general, this is an ill-posed transformation, but was made more robust by defining a fixed number of signal components (two or three) and defining each component as a Gaussian shape in a logarithmically spaced T_2 domain. This method has been previously described by Stanisz *et al.* (27) and, compared to more general approaches (23), has the benefit of producing a specified number of signals components with well-defined integrated amplitudes in the presence of spectral overlap. For comparison, T_2 spectra were also computed from S_{CPMG} data using a non-negative least-squares algorithm (22) with minimum curvature regularization (23) (NNLS-MC) that was adjusted by the generalized cross-validation method (32). This more general approach fits echo magnitudes to decaying exponential functions across a wide range of time constants and does not make any assumptions about the number of spectral peaks.

The multiple Gaussian-component fitting was performed using a separable least-squares approach (33), which utilized standard nonlinear regression of the two or three component mean T_2 values and a constant offset interleaved with an linear regression step to estimate the corresponding component amplitudes. For the S_{CPMG} fitting, no constraints were applied to the fitted parameters. For the S_{IREX} fitting, component mean T_2 values for a given sample were constrained to be equal across the different mixing times and to be within ±20% of the mean T_2 values fitted from S_{CPMG} from the same sample. Also, for S_{IREX} fitting, the amplitude of the myelin water component was allowed to be positive or negative (since IR-preparation did not exactly null this signal component), while the longer T_2 signal components were constrained to be non-negative in amplitude. The standard deviations (SDs) of the residuals to the fits of S_{CPMG} and S_{IREX} over the last 50 echo times were used as estimates of the added noise to each signal.

The estimated T_2 component amplitudes fitted from S_{CPMG} and S_{IREX} provided values for $\mathbf{P}_{CPMG}$ and $\mathbf{P}_{IREX}$, respectively, while the mean component T_2s from the CPMG measurement provided values for $\mathbf{T}_{2obs}$. In theory, these values can be simultaneously fitted with Eq. [4], Eq. [6], and the negative reciprocal eigenvalues of $\mathbf{L}_2$ to provide estimates of the 11 independent model parameters ($M_{0,a/b/c}$, $T_{1,a/b/c}$, $T_{2,a/b/c}$, k_{ab}, and k_{ac}); however, such a fitting is computational demanding. Therefore, starting with $\mathbf{P}_{CPMG}$ and $\mathbf{T}_{2obs}$ as estimates of intrinsic compartmental model parameters $\mathbf{M}_0$ and $\mathbf{T}_2$, the remaining five model parameters ($T_{1,a/b/c}$, k_{ab}, and k_{ac}) were estimated by fitting $\mathbf{P}_{IREX}$ with Eq. [6] by nonlinear regression. The resulting estimates of k_{ab} and k_{ac} were then used in Eqs. [2] and [4] to provide updated estimates of $\mathbf{M}_0$ and $\mathbf{T}_2$ by a secondary nonlinear regression step. This process was repeated until all parameters converged to a stable solution. To ensure that a global minimum was found, the whole process was repeated 50 times with randomly varied initial estimates of $T_{1,a/b/c}$, k_{ab}, and k_{ac}. Finally, the myelin water lifetime, defined as the reciprocal of the sum of the rate constants of water moving out of compartment *a*, was computed as $\tau_{myelin} = (k_{ab} + k_{ac})^{-1}$.

Given the complexity of the model and analysis, a Monte Carlo approach was used to evaluate propagation of error from measured echo amplitudes to fitted model parameters. Fitted S_{CPMG} and S_{IREX} signals from typical optic and sciatic nerve samples were used as noiseless synthetic data. Added to these data were randomly generated zero-mean Gaussian noise data with SDs as determined from the fit residuals (above) from the sample with the lowest SNR (for the each nerve type). These noisy synthetic signals were then used to estimate model parameters as described above. The process was repeated with 500 independent noise realizations to estimate the uncertainty in $\mathbf{P}_{IREX}$ data and each fitted model parameter.

RESULTS

In all cases, the equilibrium S_{CPMG} from optic nerve samples were better fitted ($p < 0.05$) with three Gaussian-shaped components than with two, as determined by the relative change in the χ^2 fit statistics tested against an *F*-distribution (34). Thus, optic nerve, like sciatic nerve, was analyzed in terms of a three-compartment model. For all sciatic nerve samples and all optic nerve samples studied at 9.4 T, the S_{CPMG} signals before and after the IR-REXSY acquisitions showed little change in the fitted T_2s (mean/max absolute change of 5/16.6% across all samples and components), indicating stable T_2 relaxation characteristics throughout the S_{IREX} acquisition. Two of the three optic nerve measurements at 4.7 T showed substantial changes (mean/max absolute change of 27.4/57.1%) and, therefore, were not included in subsequent analysis.

Representative equilibrium T_2 spectra (left) and corresponding residuals of the T_2 spectral fit (right) are shown for optic and sciatic nerve samples in Figs. 3 and 4 respectively. The top panels of each figure show T_2 spectra and fit residuals resulting from the fitting of all equilibrium CPMG echoes using the NNLS-MC method. The lower panels show similar results from the fit of equilibrium CPMG data over the restricted t_E domain (6–350 ms for optic nerve, 6–800 ms for sciatic nerve) with three Gaussian-shaped T_2 components. For both nerve types, the Gaussian component fits replicate the NNLS-MC well within the T_2 domains of 5–200 ms (optic) and 5–400 ms (sciatic), while avoiding extraneous signals outside these domains. The fitted spectra also agree well with previous studies of transverse relaxation in optic (8, 26, 27) and sciatic (26, 35–37) nerves *ex vivo*. The residuals (normalized to the first echo amplitude) show little structure, particularly near the end of the echo-train, which supports their use for characterizing the added noise as described above. The mean square fit error was 15% larger on average (across samples) for the Gaussian-component fitting over the reduced t_E domain compared with the NNLS-MC fitting over the full t_E domain. These poorer fits result from not fully accounting for the extraneous signals, particularly in the very short T_2 domain. Table 1 summarizes the fitted component amplitudes and mean T_2s as well as range of SNRs (defined as the maximum echo magnitude divided by the SD of the added noise).

The IR-REXSY data are summarized in Fig. 5 and Table 2. Figure 5 shows representative P_{IREX} data and model-predicted curves for each of the three T_2 components for both sciatic nerve (left) and optic nerve (right). For both cases, the Monte Carlo estimated error bars are not visible because they are smaller than the size of the data marker. Table 2 summarizes the mean fitted model parameters for both nerve types. Also shown is the inter-sample SD and the Monte-Carlo estimated SD for each fitted parameter. The Monte Carlo estimates demonstrate that the effect of the propagation of error on each fitted parameter (computed with the worst-case noise level for each nerve type) is similar in magnitude to the inter-sample SD. Thus we can conclude that the SNR obtained for the current experiments was sufficient to fit all model parameters, subject to the limitations of the model (see *Discussion*). In particular, Fig. 5 also shows that residuals to the fits were structured with amplitudes on order of a few percent of the P_{IREX} signals, which demonstrates small systematic misfits of the data and model. Not apparent from in this figure, although more apparent in Tables 1 and 2, is the somewhat larger inter-sample variance in fitted amplitudes of the two longer T_2 components for optic nerve compared to sciatic nerve. This likely reflects the inherent difficulty for T_2 relaxometry to distinguish intra- and extra-axonal water in optic nerve. Thus, while the relationship between the three model compartments and micro-anatomy is well supported for sciatic nerve, distinguishing the contributions of intra- and extra-axonal environments to the observed signal components in optic nerve should be made more cautiously.

For the individual sciatic and optic nerves studied at both B_0 fields, shorter T_2s and a longer T_1s were observed at 9.4 T compared to at 4.7 T, but the fitted exchange rates were similar, as expected: τ_{myelin} = 153/139 ms (optic nerve) and 2250/2210 ms (sciatic) at 4.7/9.4T, indicating no systematic difference in evaluating the samples at different B_0 fields.

DISCUSSION

Recent *ex vivo* (6) and *in vivo* (7) studies of transverse relaxation in rat spinal cord revealed a substantial variation in MWF between different white matter tracts with similar myelin content. Computational models derived from light microscopy sections (7) indicated that differing rates of inter-compartmental water exchange between these tracts might explain the observed variation in MWF. Water exchange was predicted to be faster in tracts with smaller axons and thinner myelin sheaths compared to tracts with larger axons and thicker myelin sheaths. More recently, *in vivo* studies of human brain have postulated a similar mechanism may be responsible for variations in observed water T_2 spectra in various white matter tracts (38). In these previous studies, the effect of water exchange was inferred or suspected indirectly by the experimental observations of transverse relaxation. Here, a more direct experimental approach based on relaxation exchange spectroscopy (13) is used to observe and quantify inter-compartmental water exchange in freshly excised sciatic and optic nerves.

Qualitatively, Fig. 5 demonstrates water exchanging into myelin from nonmyelin regions in sciatic and optic nerve as a function of mixing time. Note that, because of the phase-cycle employed, only water exchange during the mixing period can cause the myelin water signal magnitude to increase. To better appreciate the much faster exchange rate in the optic compared to sciatic nerves, note that the myelin water signal in the optic nerve initially increases by ≈10% of the total water signal at the minimum mixing time (that is, the total longitudinal magnetization remaining after the IR preparation) before decreasing due to longitudinal relaxation. In contrast, the sciatic nerve myelin signal increases to only a few percent of the total water signal at the minimum mixing time, suggesting a much slower initial rise due to exchange.

Quantitatively, the fitted results in Table 2 reveal a myelin water lifetime for sciatic nerve that is ≈15× greater than that of optic nerve, which we postulate is primarily due to its characteristically thicker myelin sheaths. Area-weighted mean myelin sheath thicknesses, as measured manually from the light micrographs in Fig. 6 (6, 7), were ≈0.3 and ≈1.7 μm for optic and sciatic nerve, respectively. If exchange is limited by the boundary permeability between the myelin and nonmyelin compartments, then the myelin water lifetime is proportional to the ratio of the myelin volume to the inter-compartmental boundary surface area, which is proportional to myelin thickness. In this case, we would expect lifetimes in sciatic nerve to be ≈5.6× longer than in optic nerve. Alternatively, if exchange is limited by the permeability of each lipid bilayer comprising the myelin, which is akin to saying that exchange is limited by the radial diffusion coefficient of water in the myelin, then one might crudely expect myelin water lifetime to vary with the square of the myelin thickness (mean squared displacement being proportional to time). In this case, we would expect lifetimes in sciatic nerve to be ≈32× longer than in optic nerve. Note that a single time constant is insufficient to characterize water exchange in the case of diffusion-limited exchange; therefore, the models derived from the Bloch-McConnell equations, which assume well-mixed compartments, do not fully describe water exchange under these conditions.

In the case of diffusion-limited exchange, one can alternatively consider the water between each bilayer as an individual, well-mixed compartment using a formalism similar to that described in the *Theory* section. In round numbers (estimated from (39)), these water compartments are 3 nm (optic nerve) or 4 nm (sciatic nerve) thick, separated by 5 nm thick

permeable barriers (lipid bilayers) with permeability to water of P_{lipid}. As above, the exchange rate constant of water out of each compartment can be computed as the permeability times the surface-area to volume ratio. Defining all compartments for a given myelin sheath be full of water at time $t = 0$, and ignoring water moving into the myelin, then the total amount of water remaining in the myelin as a function of time is characterized by an equation similar to Eq. [1] without the relaxation terms. Solutions with $P_{lipid} = 2.9$ μm/ms yield an apparent $\tau_{myelin} = 132$ ms and 2150 ms, respectively, for total myelin sheath thicknesses matching the optic (0.3 μm) and sciatic nerve (1.7μm), respectively. These results are roughly consistent with the mean fitted values of $\tau_{myelin} = 138$ ms and 2046 ms, as measured by IR-REXSY, suggesting that the difference in their relative sizes is due to differences in myelin thickness between optic and sciatic nerves. Of course the actual P_{lipid} of the membranes that make up myelin is not known, but $P_{lipid} = 2.9$ μm/ms is consistent with, and even on the low end of, previously reported water permeability in biological membranes (40).

The mean value of $\tau_{myelin} = 138$ ms in optic nerve reported here is similar to the $\tau_{myelin} = 161$ ms reported by a previous *ex vivo* optic nerve study by Stanisz *et al.* (8), although approximately two-fold shorter than $\tau_{myelin} = 310$ ms reported by Bjarnason *et al.* (9) in bovine white matter *ex vivo* at 24 °C. The Bjarnason study also found approximately 2× decrease in τ_{myelin} by increasing the temperature of the *ex vivo* sample to 37 °C. Applying the same factor to the present *ex vivo* data, we predict $\tau_{myelin} \approx 70$ ms in optic nerve at 37 °C. This value is in the range of apparent myelin water lifetimes (43–150 ms) *in vivo* in rat spinal cord predicted by Harkins *et al.* (7), although still somewhat long considering that the smallest mean myelin thickness in the spinal cord study was 0.43 μm compared with 0.3 μm for the optic nerves studied here. Likewise, the value of $P_{lipid} = 2.9$ μm/ms (above) is somewhat lower than the range of values predicted from the same rat spinal cord study. One interpretation of the discrepancy between the water exchange rates predicted by Harkins *et al.* and the present study is that exchange is faster *in vivo* due to more than a temperature dependent increase in the rate of water diffusion. Finally, while there are no previously published values of myelin water lifetimes in peripheral nerve with which to compare the present observations, the measured $\tau_{myelin} \approx 2$ s is in agreement with a previous assertion that water exchange is very slow in peripheral nerve (37).

In terms of the effect of water exchange on MWF measurements, the data presented here show ≈13% underestimation of MWF in optic nerve at room temperature (compare $P_{CPMG,a}$ in Table 1 to $M_{0,a}$ in Table 2). Again, extrapolating to the *in vivo* case is an open question, but using the aforementioned factor of 2× in exchange rates and model parameters for optic nerve in Table 2, one can calculate a MWF underestimation of ≈25% for optic nerve *in vivo*. This value is shy of the ≈50% predicted by Harkins *et al.* for the dorsal cortical spinal tract in rats, but still substantial compared to other studies that have indicated no effect of water exchange on measured MWF. Also, at lower B_0 (compared to the 9.4 T used for the optic nerve studies here) T_2s will be longer and relatively more affected by water exchange. While one might see underestimation of MWF as a shortcoming of myelin water imaging based on multi-exponential transverse relaxation, it also means that the water T_2 spectrum of white matter contains microstructural information related to myelin thickness.

Another potential implication of relatively short myelin water lifetimes is on microstructural inference from diffusion weighted imaging (DWI). Most quantitative models of water diffusion in white matter (see the recent summary by Panagiotaki *et al.* (41)) treat intra-axonal water as fully restricted over typical diffusion-times (10–50 ms) and neglect the presence of myelin all together. At least two such models have demonstrated the ability of DWI with varied gradient strengths and diffusion times to measure axon diameters (42, 43). The present findings raise the question of how these models are affected by inter-

compartmental water exchange, and whether appropriate DWI studies might also be sensitive to myelin thickness.

Although the relative exchange lifetimes fitted from sciatic and optic nerve were consistent with their different microanatomies, and the Monte Carlo analysis indicated that the data were acquired with sufficient SNR to fit the model parameters, several limitations of the model used herein need to be addressed. As shown in Fig. 5, some systematic differences were observed between the model and the measured P_{IREX} signals, indicating that the model is not fully describing the data. Likely causes for these deviation include (*i*) inappropriate compartment-component model assignments (i.e., the compartmental model of transverse relaxation in myelinated tissue), (*ii*) the treatment of certain model parameters as discrete, rather than continuous distributions (as was done for the T_2 spectral fitting), and (*iii*) magnetization transfer (MT) between water and MM protons within each anatomical compartment. Ultimately, the results and conclusions presented here are meaningful only in the context of the model used, so we consider below the potential model shortcomings in more detail.

Regarding point (*i*), because the inversion of exponentially decaying data to a spectrum of T_2 component amplitudes is generally ill posed, some assumptions about the model are required for any meaningful interpretation of the data. Although compartmental modeling of the ^{1}H NMR signal in myelinated tissue is an ongoing area of research, the compartment-component relationships used here were based upon a sizeable body of literature (3–6, 24–26) and represents the most well supported explanation of multi-exponential transverse relaxation in myelinated tissues. Regarding point (*ii*), previous work (7) found that incorporating microanatomical heterogeneity into a model of water diffusion and relaxation in WM provided better fits to experimental observations than did a Bloch-McConnell model based on three discrete compartments. Such an approach to IR-REXSY analysis would be computationally demanding, but might also better describe experimental data, particularly in cases where tissues with similar mean axon dimensions but widely different distribution of sizes were being compared. In the present case, the microstructural differences between optic and sciatic nerve are stark enough that the inclusion of microscopic heterogeneity is unlikely to change the conclusion that water exchange is much faster in optic nerve than sciatic nerve, although it might affect the absolute values of fitted model parameters.

Finally, with regards to point (*iii*), the model used here considers only magnetization from water, although it is well known that there is a significant MT effect between water and MM protons in myelinated tissues (8, 9, 37). In fact, inverting longitudinal magnetization of water protons while leaving MM magnetization near equilibrium results in a distinctly bi-exponential relaxation of the water longitudinal magnetization, which is the basis for some quantitative magnetization transfer imaging methods (44). Without *a priori* knowledge of MM proton T_2 and lineshape, the relative contribution of saturation and rotation effects of RF pulses on the MM longitudinal magnetization ($M_{z,MM}$) is unclear. If we assume pure saturation, the high power 90°–180°–90° pulses in the 'EXCITE' period (see Fig. 1) will drive the MM longitudinal magnetization toward, but not below, zero ($M_{z,MM} \geq 0$). If, however, we assume pure rotation, the MM magnetization will be rotated into the transverse by the first 90° pulse in the 'EXCITE' period and then filtered out because $t_{E1} >> T_{2,MM}$. Combining these effects, one can assume that $M_{z,MM} \geq 0$ at the beginning of the IR-REXSY mixing period. At the same time, because the myelin water nulls at a shorter t_1 that the other signal components, the longitudinal magnetization of the nonmyelin water pools will be < 0 at the onset of the mixing period. Thus, exchange between myelin water and MM protons during the mixing period will either be small (if $M_{z,MM} \approx 0$ when $M_{z,MyelinWater} \approx 0$) or will tend to compete with exchange between myelin water and nonmyelin water compartments (if $M_{z,MM} > 0$ when $M_{z,NonmyelinWater} < 0$), resulting in only overestimations

of τ_{myelin}. Thus, we reason that MT effects on the IR-REXSY studies here should be small and are unlikely to explain the relatively large differences in τ_{myelin} found in optic nerve compared to sciatic nerve.

CONCLUSIONS

Relaxation exchange spectroscopy was used to provide novel and direct observations of inter-compartmental water exchange in freshly excised rat optic nerve and frog sciatic nerve samples. In the optic nerve samples, the measured τ_{myelin} values were similar to those from a previous report in bovine optic nerve *ex vivo*, but significantly shorter than others reported from cerebral white matter. Extrapolation of the present results to *in vivo* temperatures supports previous reports that inter-compartmental water significantly alters water proton transverse relaxation in white matter. In sciatic nerve, the measured τ_{myelin} values were much longer, consistent with the interpretation τ_{myelin} is largely dictated by the myelin sheath thickness. These findings offer the potential for the development of novel MRI methods for characterizing myelin thickness.

Acknowledgments

We thank the Vanderbilt Electron Microscopy Core for histological processing and Bill Valentine for microscope resources.

Grant sponsors: NIH R01 EB001744, NIH R01 EB000461, and NSF Career Award 0448915

REFERENCES

1. Vasilescu V, Katona E, Simplaceanu V, Demco D. Water compartments in myelinated nerve. 3. Pulsed NMR results. Experientia. 1978; 34(11):1443–1444. [PubMed: 309823]
2. Menon RS, Rusinko MS, Allen PS. Proton relaxation studies of water compartmentalization in a model neurological system. Magn Reson Med. 1992; 28(2):264–274. [PubMed: 1281258]
3. Mackay A, Whittal K, Adler J, Li D, Paty D, Graeb D. In-vivo visualization of myelin water in brain by magnetic resonance. Magn Reson Med. 1994; 31(6):673–677. [PubMed: 8057820]
4. Stewart WA, Mackay AL, Whittall KP, Moore GRW, Paty DW. Spin-spin relaxation in experimental allergic encephalomyelitis: Analysis of CPMG data using a nonlinear least-squares method and linear inverse-theory. Magn Reson Med. 1993; 29(6):767–775. [PubMed: 8350719]
5. Laule C, Leung E, Lis DK, Traboulsee AL, Paty DW, MacKay AL, Moore GR. Myelin water imaging in multiple sclerosis: quantitative correlations with histopathology. Mult Scler. 2006; 12(6):747–753. [PubMed: 17263002]
6. Dula AN, Gochberg DF, Valentine HL, Valentine WM, Does MD. Multiexponential T2, magnetization transfer, and quantitative histology in white matter tracts of rat spinal cord. Magn Reson Med. 2010; 63(4):902–909. [PubMed: 20373391]
7. Harkins KD, Dula AN, Does MD. Effect of inter-compartmental water exchange on the apparent myelin water fraction in multiexponential T(2) measurements of rat spinal cord. Magn Reson Med. 2011
8. Stanisz G, Kecojevic A, Bronskill M, Henkelman R. Characterizing white matter with magnetization transfer and T2. Magn Reson Med. 1999; 42(6):1128–1136. [PubMed: 10571935]
9. Bjarnason TA, Vavasour IM, Chia CL, MacKay AL. Characterization of the NMR behavior of white matter in bovine brain. Magn Reson Med. 2005; 54(5):1072–1081. [PubMed: 16200557]
10. Kalantari S, Laule C, Bjarnason TA, Vavasour IM, MacKay AL. Insight into in vivo magnetization exchange in human white matter regions. Magn Reson Med. 2011; 66(4):1142–1151. [PubMed: 21381107]
11. Lee JH, Labadie C, Springer CS, Harbison GS. 2-Dimensional Inverse Laplace Transform Nmr - Altered Relaxation-Times Allow Detection of Exchange-Correlation. J Am Chem Soc. 1993; 115(17):7761–7764.

12. Washburn KE, Callaghan PT. Tracking pore to pore exchange using relaxation exchange spectroscopy. Phys Rev Lett. 2006; 97(17):175502. [PubMed: 17155481]
13. Dortch RD, Horch RA, Does MD. Development, simulation, and validation of NMR relaxation-based exchange measurements. J Chem Phys. 2009; 131(16):164502. [PubMed: 19894951]
14. McDonald PJ, Korb JP, Mitchell J, Monteilhet L. Surface relaxation and chemical exchange in hydrating cement pastes: a two-dimensional NMR relaxation study. Phys Rev E Stat Nonlin Soft Matter Phys. 2005; 72(1 Pt 1):011409. [PubMed: 16089963]
15. McDonald PJ, Mitchell J, Mulheron M, Monteilhet L, Korb JP. Two-dimensional correlation relaxation studies of cement pastes. Magn Reson Imaging. 2007; 25(4):470–473. [PubMed: 17466766]
16. Monteilhet L, Korb JP, Mitchell J, McDonald PJ. Observation of exchange of micropore water in cement pastes by two-dimensional T(2)-T(2) nuclear magnetic resonance relaxometry. Phys Rev E Stat Nonlin Soft Matter Phys. 2006; 74(6 Pt 1):061404. [PubMed: 17280070]
17. Mitchell J, Griffith JD, Collins JH, Sederman AJ, Gladden LF, Johns ML. Validation of NMR relaxation exchange time measurements in porous media. J Chem Phys. 2007; 127(23):234701. [PubMed: 18154403]
18. Sun C, Boutis GS. Measurement of the exchange rate of waters of hydration in elastin by 2D *T*2–*T*2 correlation nuclear magnetic resonance spectroscopy. New J. Phys. 2011; 13(2):025026.
19. Carr HY, Purcell EM. Effects of Diffusion on Free Precession in Nuclear Magnetic Resonance Experiments. Physical Review. 1954; 94(3):630.
20. Meiboom S, Gill D. Modified spin echo method for measuring nuclear relaxation times. The Review of Scientific Instruments. 1958; 29(8):688–691.
21. McConnell MH. Reaction Rates by Nuclear Magnetic Resonance. J Chem Phys. 1958; 28(3):430–431.
22. Lawson, CL.; Hanson, RJ. Solving least squares problems. Englewood Cliffs, NJ: Prentice-Hall; 1974.
23. Whittall KP, Mackay AL. Quantitative Interpretation of NMR Relaxation Data. J Magn Reson. 1989; 84(1):134–152.
24. Peled S, Cory DG, Raymond SA, Kirschner DA, Jolesz FA. Water diffusion, T2, and compartmentation in frog sciatic nerve. Magn Reson Med. 1999; 42(5):911–918. [PubMed: 10542350]
25. Wachowicz K, Snyder RE. Assignment of the T2 components of amphibian peripheral nerve to their microanatomical compartments. Magn Reson Med. 2002; 47(2):239–245. [PubMed: 11810666]
26. Dortch RD, Apker GA, Valentine WM, Lai B, Does MD. Compartment-specific enhancement of white matter and nerve ex vivo using chromium. Magn Reson Med. 2010; 64(3):688–697. [PubMed: 20806376]
27. Stanisz GJ, Henkelman RM. Diffusional anisotropy of T2 components in bovine optic nerve. Magn Reson Med. 1998; 40(3):405–410. [PubMed: 9727943]
28. Bonilla I, Snyder RE. Transverse relaxation in rat optic nerve. NMR Biomed. 2007; 20(2):113–120. [PubMed: 16998953]
29. Horch RA, Wilkens K, Gochberg DF, Does MD. RF coil considerations for short-T2 MRI. Magn Reson Med. 2010; 64(6):1652–1657. [PubMed: 20665825]
30. Horch RA, Gore JC, Does MD. Origins of the Ultrashort-T-2 H-1 NMR Signals in Myelinated Nerve: A Direct Measure of Myelin Content? Magn Reson Med. 2011; 66(1):24–31. [PubMed: 21574183]
31. Gudbjartsson H, Patz S. The Rician distribution of noisy MRI data. Magn Reson Med. 1995; 34(6):910–914. [PubMed: 8598820]
32. Golub GH, Heath M, Wahba G. Generalized Cross-Validation as a Method for Choosing a Good Ridge Parameter. Technometrics. 1979; 21(2):215–223.
33. Golub G, Pereyra V. Separable nonlinear least squares: the variable projection method and its applications. Inverse Problems. 2003; 19(2):R1–R26.

34. Bevington, PR.; Robinson, DK. Data reduction and error analysis for the physical sciences. 3rd Edition. Crawfordsville, IN: McGraw-Hill; 2003.
35. Does MD, Snyder RE. T2 relaxation of peripheral nerve measured in-vivo. Magn Reson Imaging. 1995; 13(4):575–580. [PubMed: 7674853]
36. Does MD, Snyder RE. Multiexponential T2 relaxation in degenerating peripheral nerve. Magn Reson Med. 1996; 35(2):207–213. [PubMed: 8622585]
37. Does MD, Beaulieu C, Allen PS, Snyder RE. Multi-component T1 relaxation and magnetisation transfer in peripheral nerve. Magn Reson Imaging. 1998; 16(9):1033–1041. [PubMed: 9839987]
38. Russell-Schultz B, Laule C, Li DKB, MacKay AL. What causes the hyperintense T2-weighting and increased short T2 signal in the corticospinal tract? Magn Reson Imaging. in press.
39. Quarles, RH.; Macklin, WB.; Morell, P. Myelin Formation, Structure, and Biochemistry. In: Siegel, GJ.; Albers, RW.; Brady, ST.; Price, DL., editors. Basic Neurochemistry: Molecular, Cellular, and Medical Aspects. 7th Ed. San Diego: Academic Press; 2006. p. 52-54.
40. Weiss, TL. Cellular Biophysics, Volume 1: Transport. Cambridge MA: MIT Press; 1996. p. 238
41. Panagiotaki E, Schneider T, Siow B, Hall MG, Lythgoe MF, Alexander DC. Compartment models of the diffusion MR signal in brain white matter: a taxonomy and comparison. Neuroimage. 2012; 59(3):2241–2254. [PubMed: 22001791]
42. Assaf Y, Blumenfeld-Katzir T, Yovel Y, Basser PJ. AxCaliber: A method for measuring axon diameter distribution from diffusion MRI. Magnetic Resonance In Medicine. 2008; 59(6):1347–1354. [PubMed: 18506799]
43. Alexander DC, Hubbard PL, Hall MG, Moore EA, Ptito M, Parker GJM, Dyrby TB. Orientationally invariant indices of axon diameter and density from diffusion MRI. Neuroimage. 2010; 52(4):1374–1389. [PubMed: 20580932]
44. Gochberg DF, Gore JC. Quantitative Magnetization Transfer Imaging via Selective Inversion Recovery with Short Repetition Times. Magn Reson Med. 2007; 57:437–441. [PubMed: 17260381]

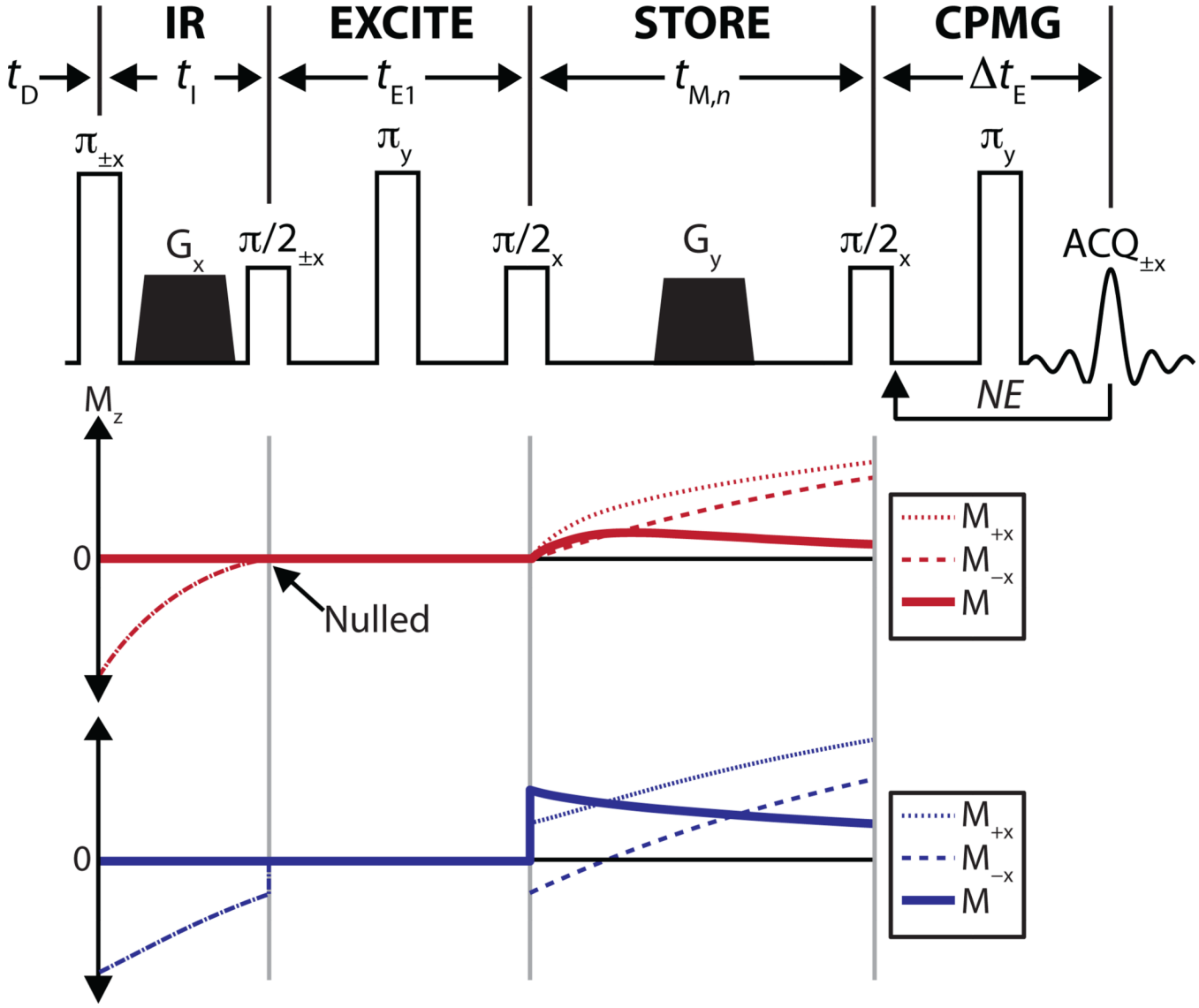

Fig. 1.

(Top) Pulse sequence diagram for the IR-REXSY sequence. To quantify exchange, a CPMG measurement is performed over a range of $t_{M,n}$ (n = 1 to NM) values with all other timings fixed. Legend: t_D = predelay, t_I = inversion time, t_{E1} = delay prior to the mixing period, $t_{M,n}$ = n^{th} mixing time, Δt_E = echo spacing of CPMG measurement, NE = number of CPMG echoes, NM = number of mixing times, ACQ = acquisition, and $G_{x,y}$ = crusher gradients applied along x or y directions. The phase each RF pulse and acquisition across the two-step phase cycle is given as a subscript (a single value is given for pulses of constant phase). (Bottom) Simulated M_z for a two-component system undergoing exchange. In these simulations, t_I has been chosen to null one of the two components. Shown are the M_z for the 1st (M_+) and 2nd step (M_-) of the phase cycle along with the final magnetization ($M = M_+ - M_-$). Note the initial increase in the magnitude of the nulled component during the mixing period, which can be directly attributed to exchange with the other component.

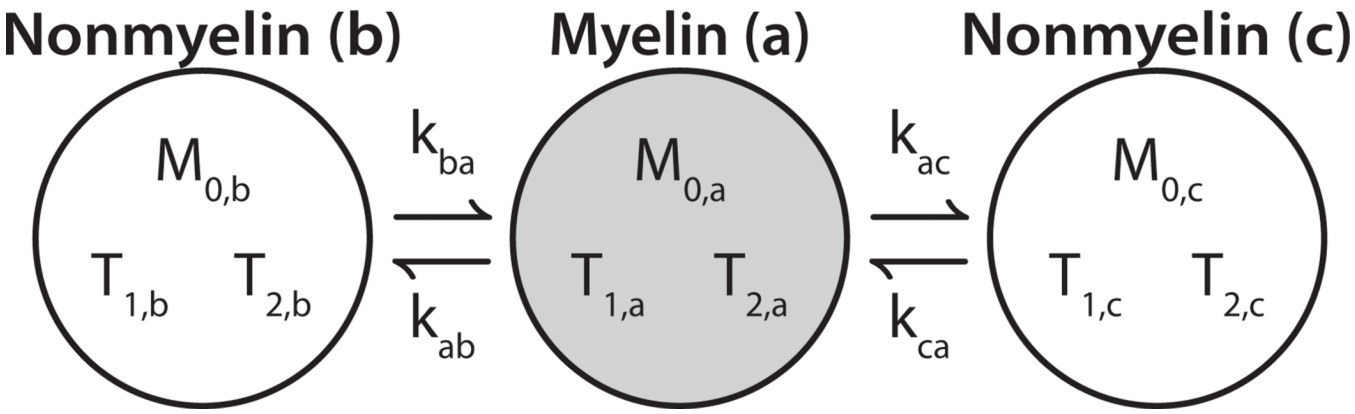

Fig. 2.

Three-compartment model of optic and sciatic nerve. The three compartments are labeled ‘a’, ‘b’, and ‘c’ in order of increasing T_2. The short-T_2 component (gray circle) represents myelin water, while the other two components (white circles) represent nonmyelin water (intra- and extra-axonal water). Because water must traverse the myelin sheath to pass between intra- and extra-axonal spaces, exchange between the nonmyelin compartments in neglected. Under the condition of equilibrium (i.e., compartment sizes are constant), this results in model defined by 11 independent parameters: three equilibrium magnetizations ($M_{0,a/b/c}$), three transverse relaxation times ($T_{2,a/b/c}$), three longitudinal relaxation times ($T_{1,a/b/c}$), and two exchange rate constants (k_{ab} and k_{ac}).

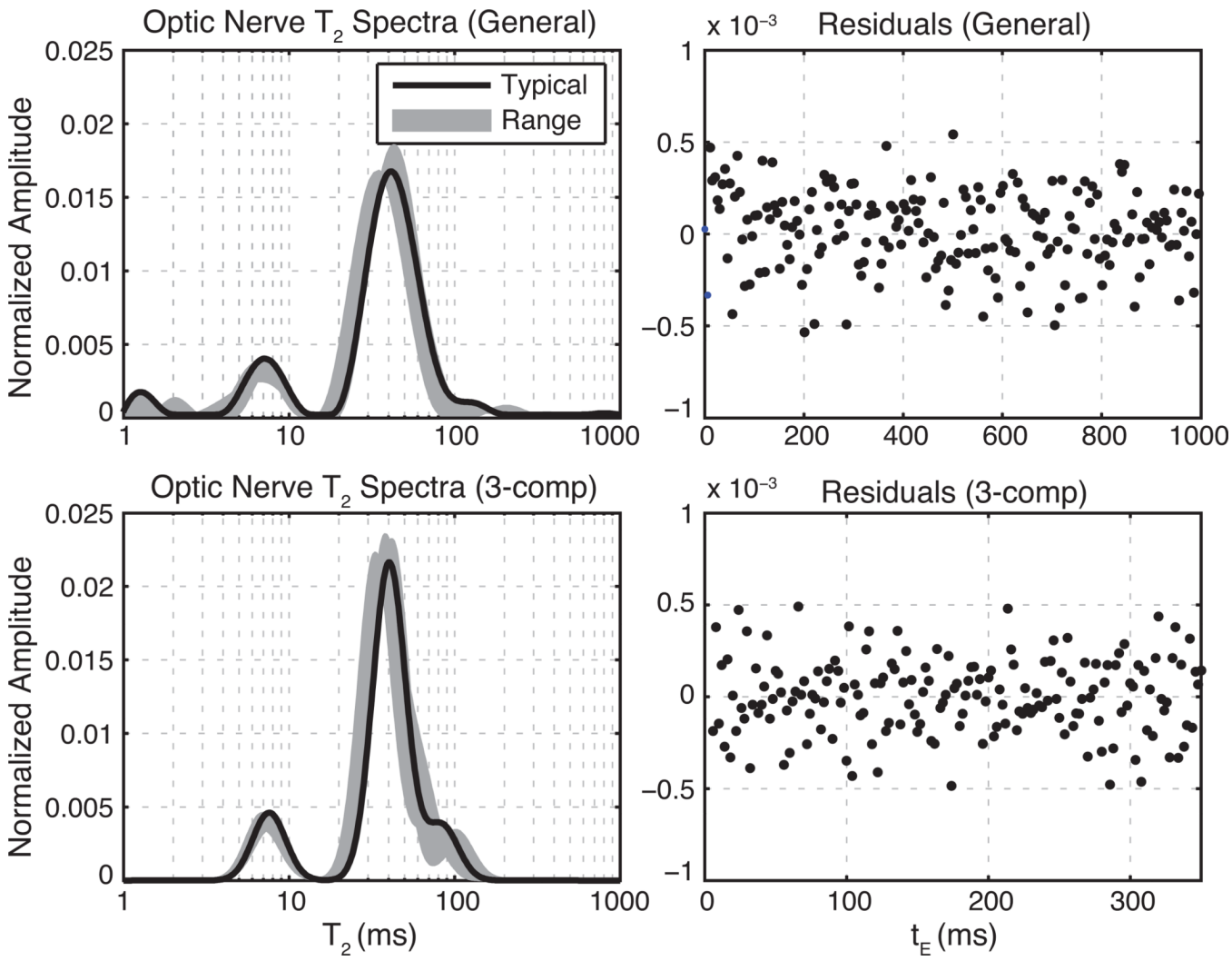

Fig. 3.

Equilibrium T_2 spectra of optic nerve at 9.4 T. Left panels show fitted T_2 spectra and right panels show residuals from a typical sample fit normalized to the maximum echo amplitude. Top panels show results of fitting the full echo train with only non-negative and minimum curvature constraints. The bottom panels show the results of fitting the truncated echo train with three Gaussian-shaped T_2 components. For clarity, only every 5^{th} residual is plotted in the upper right frame.

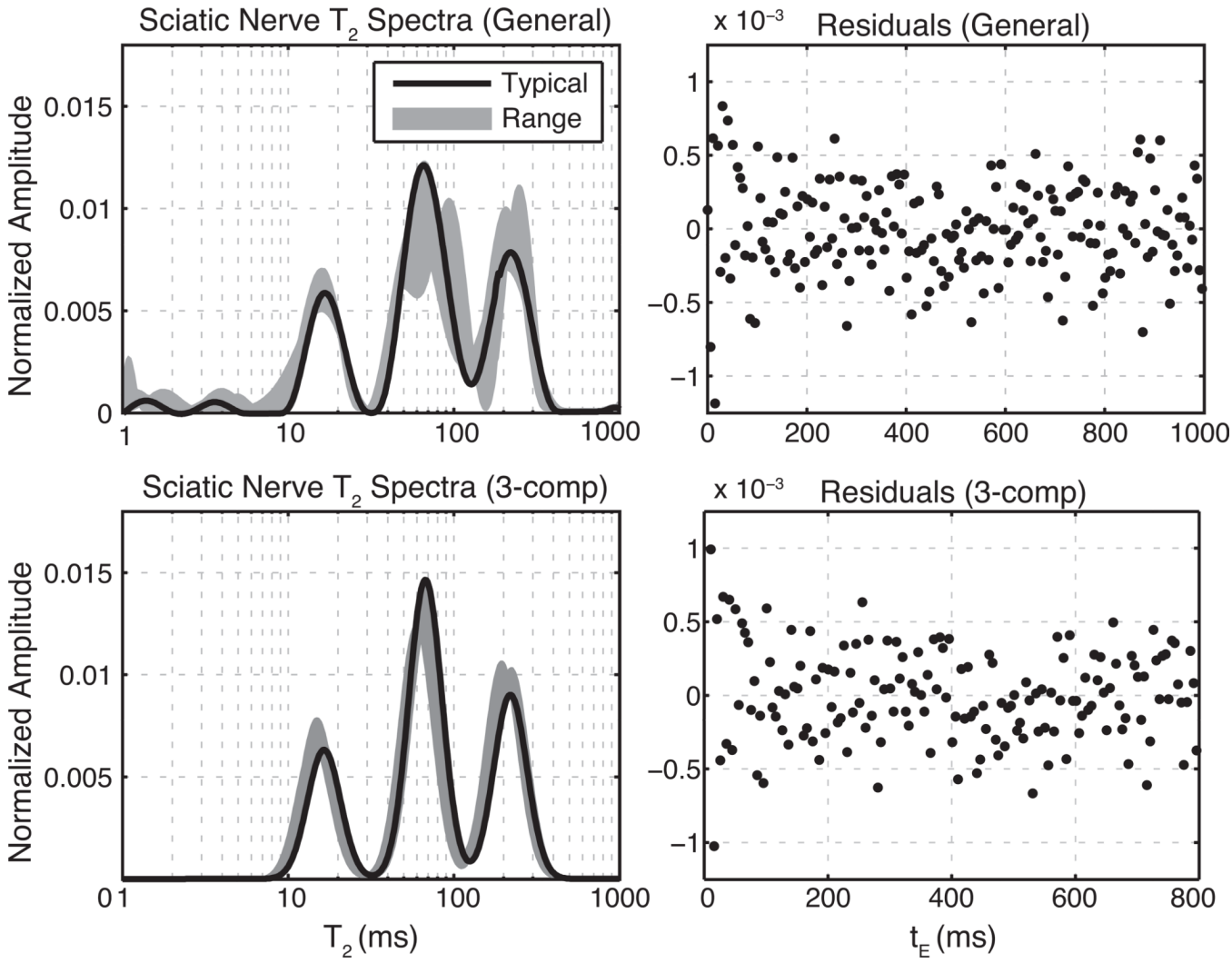

Fig. 4.

Equilibrium T_2 spectra of sciatic nerve at 4.7 T. Left panels show fitted T_2 spectra and right panels show residuals from a typical sample fit normalized to the maximum echo amplitude. Top panels show results of fitting the full echo train with only non-negative and minimum curvature constraints. The bottom panels show the results of fitting the truncated echo train with three Gaussian-shaped T_2 components. For clarity, only every 5^{th} residual is plotted in the upper and lower right frames.

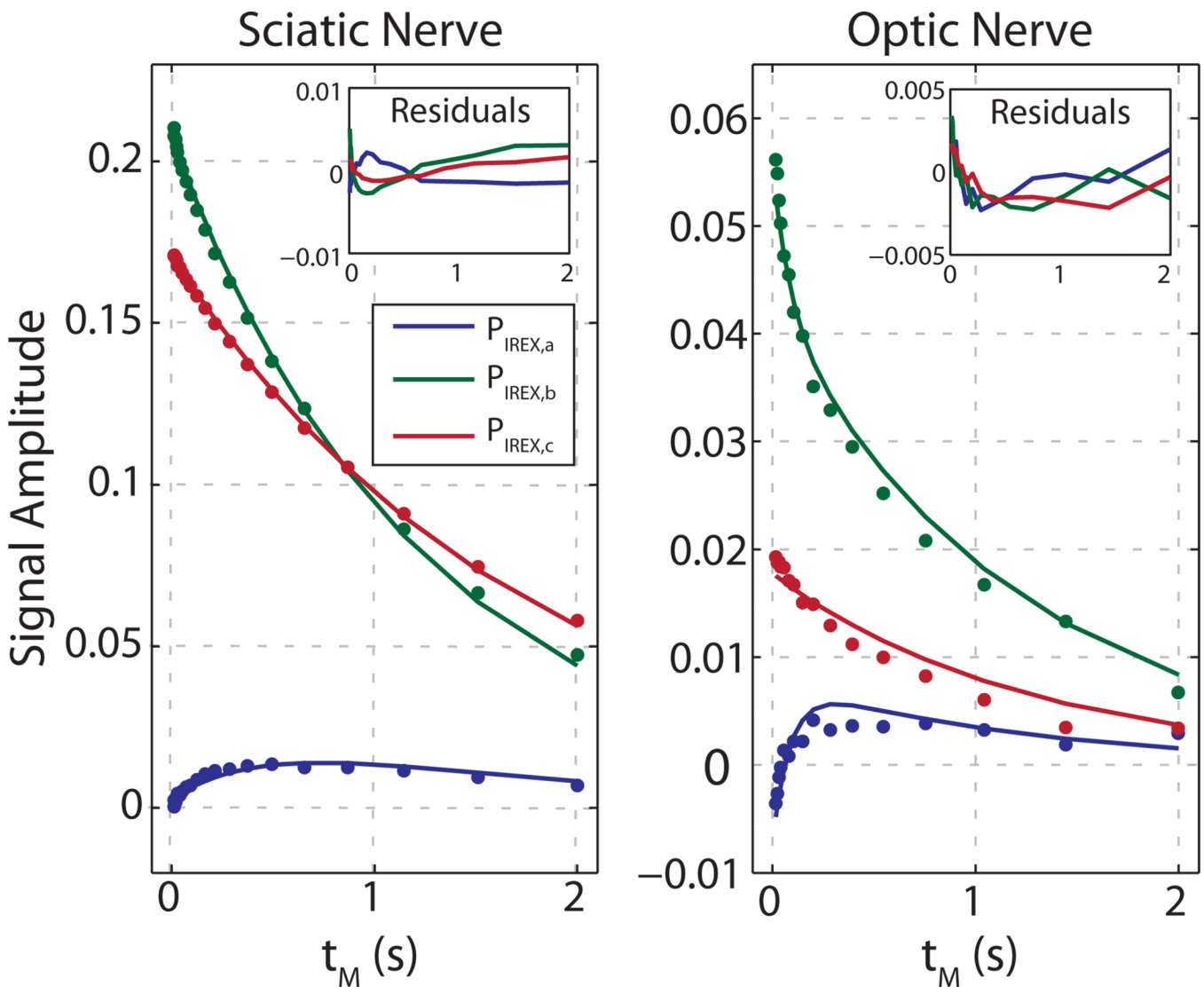

Fig. 5.

Sample IR-REXSY data (P_{IREX}) from sciatic nerve (left) and optic nerve (right). In both cases, error bars, as determined by Monte Carlo simulation for the worst case SNR across respective samples, are smaller than the data marker size.

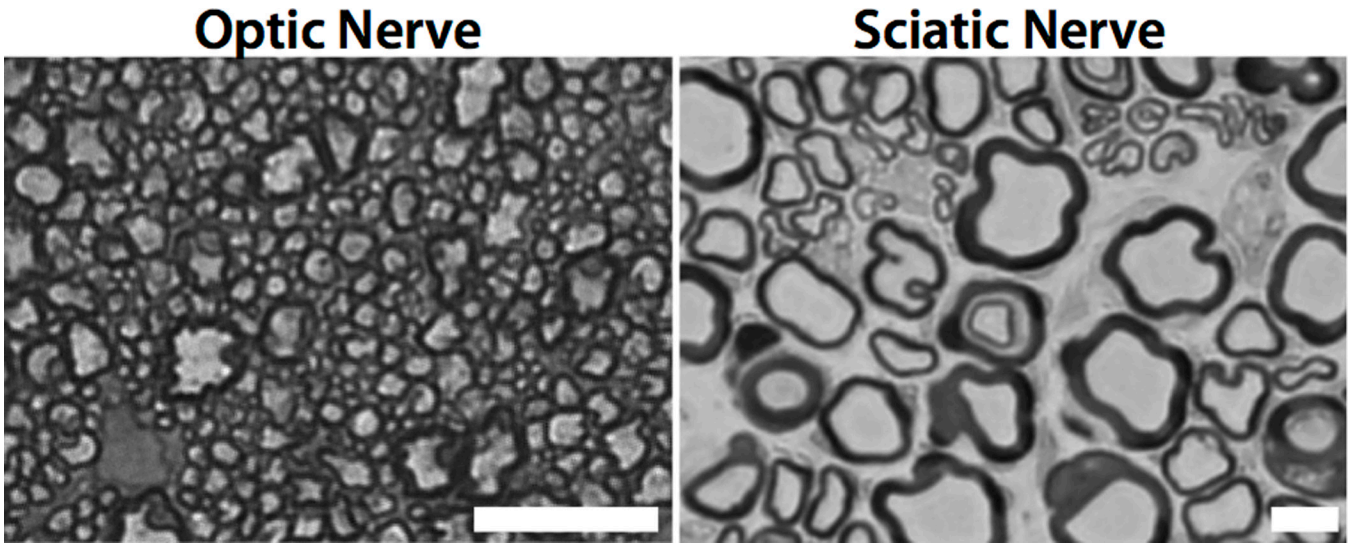

Fig. 6.
Representative light micrograph images from optic and sciatic nerve. The white scale bar = 10 μm in both frames.

Table 1

T_2 spectral characteristics from equilibrium CPMG measurements of sciatic and optic nerve. All sciatic nerve samples were scanned at 4.7 T, and all optic nerve samples were scanned at 9.4 T. Values of signal component fractions ($P_{CPMG,i}$) and mean observed T_2s ($T_{2obs,i}$) are given as the mean ± SD across samples. The three signal components are labeled $i \in$[a, b, c] in order of increasing observed T_2, with the short-T_2 component ('a') representing myelin water.

	Optic Nerve (*n* = 5)	**Sciatic Nerve (*n* = 4)**
$P_{CPMG,a}$ (%)	13.6 ± 1.9	22.9 ± 2.5
$P_{CPMG,b}$ (%)	71.3 ± 4.7	44.3 ± 3.0
$P_{CPMG,c}$ (%)	15.1 ± 5.3	32.8 ± 1.8
$T_{2obs,a}$(ms)	7.2 ± 0.2	15.6 ± 1.0
$T_{2obs,b}$(ms)	36.6 ± 2.5	65.6 ± 4.3
$T_{2obs,c}$(ms)	79.9 ± 13	212 ± 11
SNR [1]	2960-6830	3120–11000

[1] SNR of the S_{CPMG} signal. variation within a given nerve type is due to variation in sample size.

Table 2

Fitted three-compartment model values from IR-REXSY measurements in optic and sciatic nerve. All sciatic nerve samples were scanned at 4.7 T, and all optic nerve samples were scanned at 9.4 T. Values are given as the mean ± SD across samples (SD across Monte Carlo trials). For both optic and sciatic nerves, the Monte Carlo trials were generated using an SNR equal to the lowest SNR observed across samples. The three signal components are labeled $i \in$[a, b, c] in order of increasing observed T_2, with the short-T_2 component ('a') representing myelin water.

	Optic Nerve (n = 5)	**Sciatic Nerve (n = 4)**
$M_{0,a}$ (%)	15.5 ± 2.2 (0.3)	23.3 ± 2.5 (0.1)
$M_{0,b}$ (%)	69.3 ± 4.4 (6.2)	43.9 ± 3.0 (0.1)
$M_{0,c}$ (%)	14.9 ± 5.1 (6.5)	32.7 ± 1.7 (0.2)
$T_{2,a}$ (ms)	7.6 ± 0.2 (0.3)	15.7 ± 1.0 (0.1)
$T_{2,b}$ (ms)	38.6 ± 2.7 (1.3)	66.5 ± 4.3 (0.3)
$T_{2,c}$ (ms)	81.8 ± 11 (6.9)	215 ± 11 (1.2)
$T_{1,a}$ (ms)	547 ± 54 (48)	651 ± 19 (0.8)
$T_{1,b}$ (ms)	1730 ± 203 (64)	1517 ± 101 (5.8)
$T_{1,c}$ (ms)	1558 ± 86 (150)	1960 ± 107 (23)
k_{ab} (s^{-1})	6.7 ± 1.9 (0.6)	0.39 ± 0.01 (0.03)
k_{ac} (s^{-1})	0.6 ± 1.2 (3.7)	0.10 ± 0.02 (0.03)
τ_{myelin} (ms)	138 ± 15 (30)	2046 ± 140 (24)
SNR[1]	310–814	2409–5508

[1] SNR of the S_{IREX} signal. SNR variation within a given nerve type is due to variation in sample size.